Table S1. Electrocardiographic Assessment

	WT		KO	
Data	Sham (n=6)	Banding (n=6)	Sham (n=6)	Banding (n=6)
HR, bpm	508±18	518±18	512±4	526±10
P wave, ms	14.1 ± 0.2	15.3 ± 1.5	13.9 ± 1.0	16.0 ± 0.7
PQ interval, ms	45.1 ± 1.8	45.7 ± 1.3	44.6 ± 1.2	46.3 ± 0.8
QRS, ms	11.2 ± 0.6	11.9 ± 0.9	11.6 ± 1.0	11.7 ± 0.6
QT, ms	19.8 ± 0.7	24.2± 1.2*	20.8 ± 1.6	24.5 ± 0.9*

Values are expressed as means ± standard errors. *p <0.05 compared to sham.

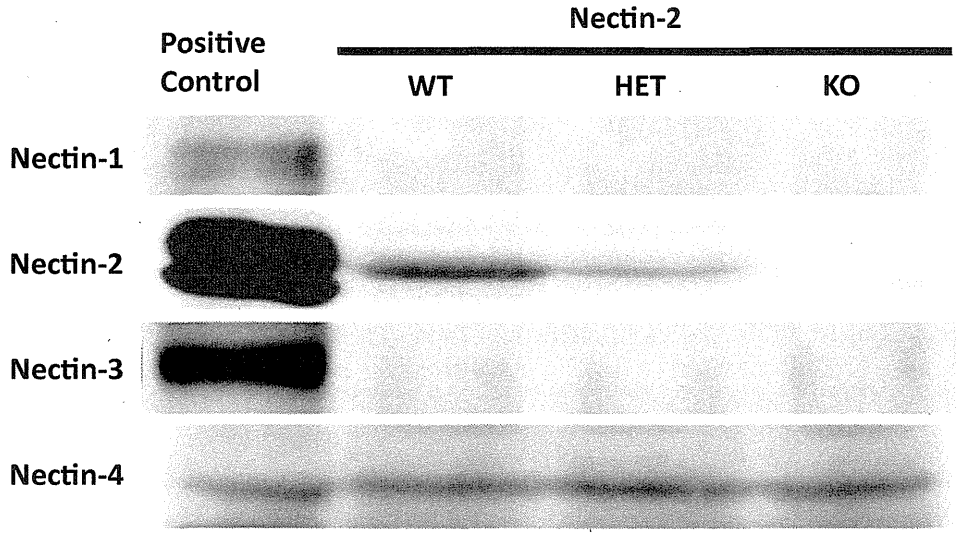

Figure S1. Expression of nectin-1and -3 in nectin-2-KO mice. Representative Western blots of nectins using the heart lysates from nectin-$2^{+/+}$ (WT), nectin-$2^{+/-}$ (HET), and nectin-$2^{-/-}$ (KO) mice. The extreme left lane showed positive control of each nectin protein. Ten μg of protein was applied to each lane.

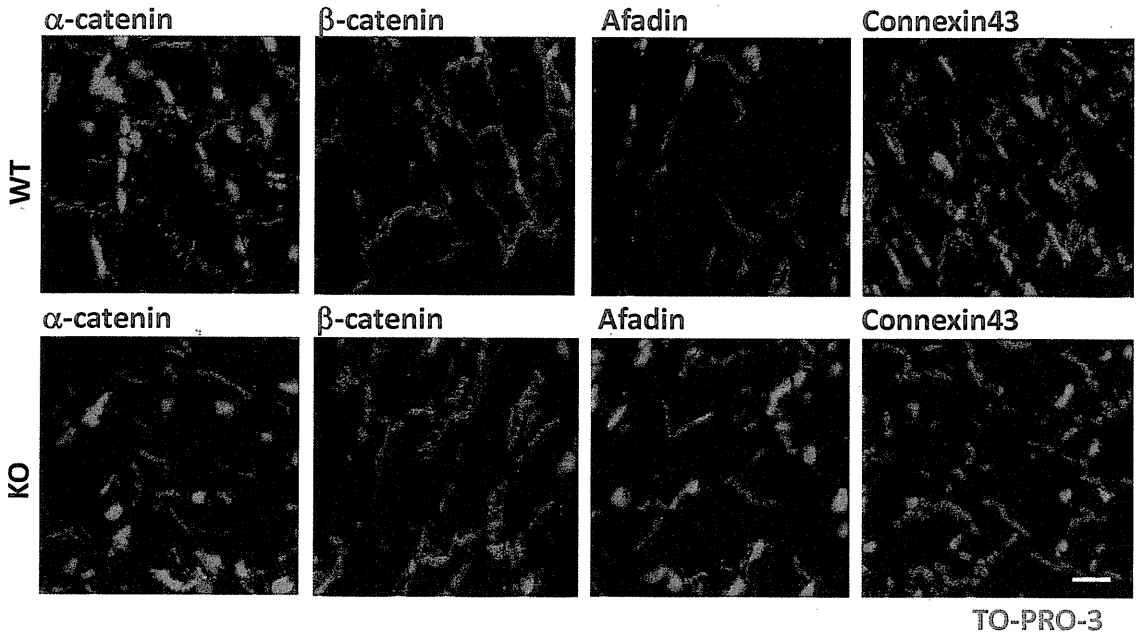

Figure S2. Distribution of intercalated disc protein in nectin-2-KO mice heart. Immunofluorescence of heart sections from WT and nectin-2-KO mice. AJ proteins, such as α-catenin, β-catenin, and afadin, and GJ protein, connexin43, were expressed normally in the intercalated discs of both WT and nectin-2-KO mice. Bar indicates 10 μm.

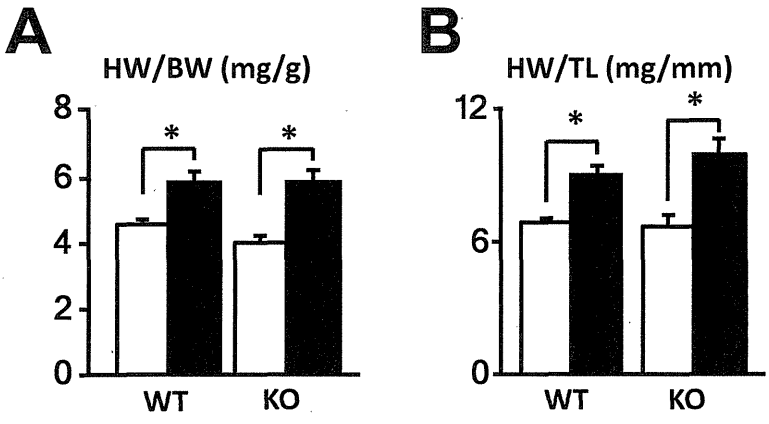

Figure S3. Cardiac hypertrophy induced by aortic banding at 4 weeks after the operation. A, HW/body weight (BW) (mg/g). B, HW/tibial length (TL) (mg/mm). White bars and black bars indicate sham-operated and aortic banding-operated mice, respectively. The degree of cardiac hypertrophy induced by aortic banding was similar in WT and nectin-2-KO mice. Numbers for each group in A and B are shown in Table 1.

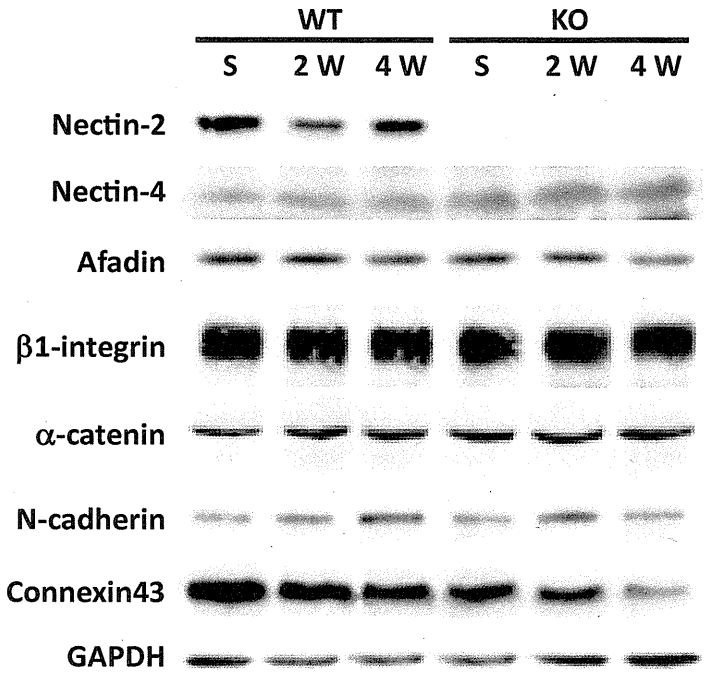

Figure S4. Changes in intercalated disc proteins under pressure overload. Representative Western blots of the molecules existing in the intercalated disc. There was no significant change in the expression of AJ proteins in both genotypes after banding. Connexin43 was significantly decreased in nectin-2-KO mice after banding. Ten μg of protein was applied to each lane.

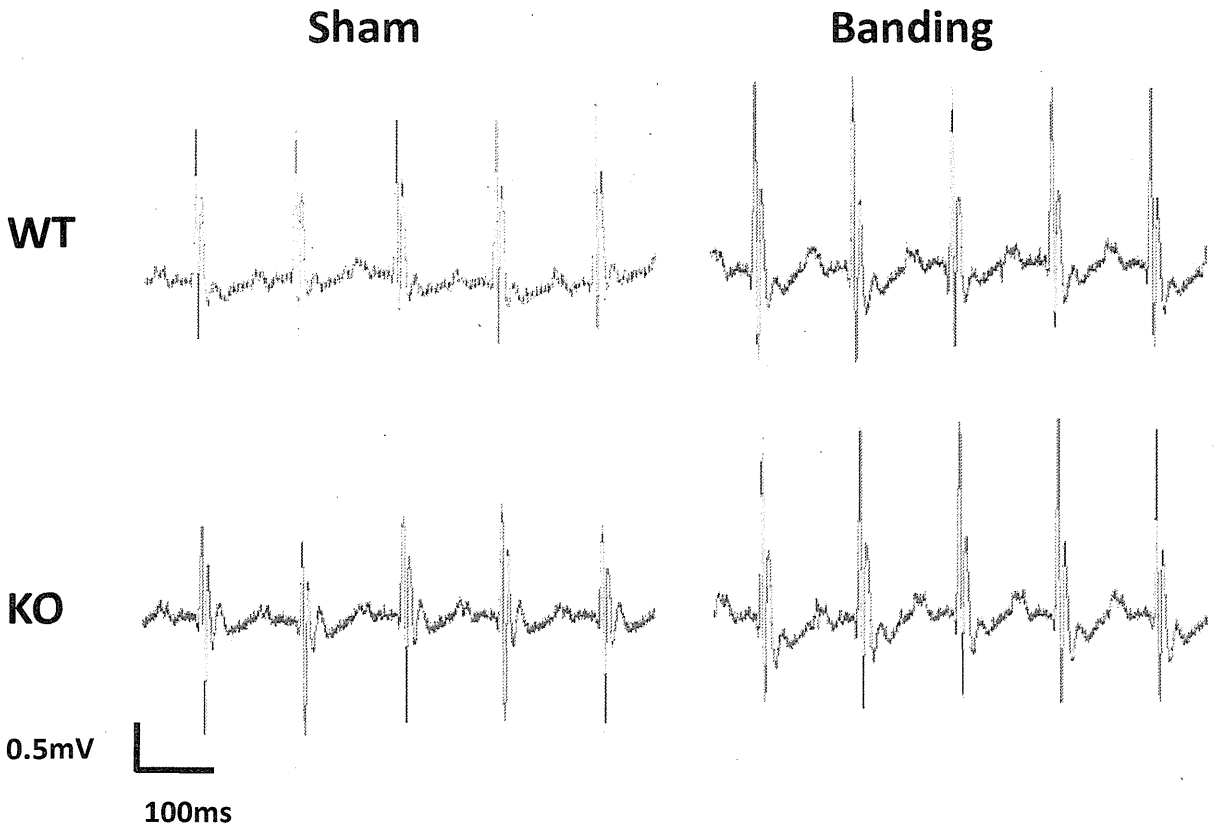

Figure S5. Echocardiogram (lead I) from WT and nectin-2-KO mice at 4 weeks after operation. No arrhythmia was detected through whole recording in both genotypes even after aortic banding.

J Physiol Sci (2011) 61:457–465
DOI 10.1007/s12576-011-0166-7

ORIGINAL PAPER

Norwood procedure with non-valved right ventricle to pulmonary artery shunt improves ventricular energetics despite the presence of diastolic regurgitation: a theoretical analysis

Shuji Shimizu · Dai Une · Toshiaki Shishido · Atsunori Kamiya · Toru Kawada · Shunji Sano · Masaru Sugimachi

Received: 17 May 2011 / Accepted: 10 July 2011 / Published online: 10 August 2011

Abstract When the Norwood procedure is conducted for the hypoplastic left heart syndrome using a non-valved right ventricle (RV) to pulmonary artery (PA) shunt, diastolic regurgitation from PA to RV may have an adverse effect on postoperative hemodynamics. In this study, we examined the impact of the diastolic regurgitation on ventricular energetics by computational analysis using a combination of a time-varying elastance chamber model and a modified three-element Windkessel vascular model. This study revealed that use of the valved or non-valved RV-PA shunt eliminated pulmonary over-circulation which was observed when using the systemic to pulmonary artery shunt (modified Blalock–Taussig shunt). Although the valved RV-PA shunt improved pulmonary blood supply and consequently increased pulmonary artery flow and oxygen saturation compared to the non-valved RV-PA shunt, the non-valved RV-PA shunt improved ventricular energetics in spite of the presence of PA to RV regurgitation.

Keywords Hypoplastic left heart syndrome · Norwood procedure · Right ventricle to pulmonary artery shunt · Ventricular energetics · Valved · Computational model

S. Shimizu (✉) · D. Une · T. Shishido · A. Kamiya · T. Kawada · M. Sugimachi
Department of Cardiovascular Dynamics, National Cerebral and Cardiovascular Center Research Institute, 5-7-1 Fujishiro-dai, Suita, Osaka 565-8565, Japan
e-mail: shujismz@ri.ncvc.go.jp

S. Shimizu · S. Sano
Department of Cardiovascular Surgery, Okayama University Graduate School of Medicine, Dentistry and Pharmaceutical Sciences, Okayama, Japan

Introduction

The outcome of the Norwood procedure for hypoplastic left heart syndrome (HLHS) has improved in the past several decades. Previously, pulmonary circulation was maintained by a systemic to pulmonary artery shunt (SPS), such as the modified Blalock–Taussig shunt. However, the SPS has the drawback of systemic-to-pulmonary diastolic run-off, which causes a massive increase in ventricular preload. The development of the right ventricle to pulmonary artery (RV-PA) shunt may have contributed to the dramatic improvement in clinical outcome of recent years, because the RV-PA shunt eliminates the diastolic run-off and increases diastolic systemic arterial pressure (SAP). This increase in diastolic SAP may improve coronary blood supply [1]. Furthermore, the RV-PA shunt may reduce myocardial oxygen demand. Bove et al. [2] reported that the RV-PA shunt decreased stroke work and improved right ventricular energetics.

The RV-PA shunt may be classified into valved and non-valved. The non-valved RV-PA shunt is associated with diastolic regurgitation from PA to RV. This regurgitation may increase RV preload and myocardial oxygen demand compared to the valved RV-PA shunt. Therefore, preventing diastolic regurgitation using the valved conduit may further improve clinical outcome. Reihartz et al. [3] reported that use of a homograft valved RV-PA conduit was associated with low early mortality. Takeuchi et al. [4] used a valved saphenous vein homograft and also reported improved right ventricular function. However, whether the non-valved RV-PA shunt truly improves the outcome of the Norwood procedure compared to the SPS, and whether the valved RV-PA shunt further improves the outcome compared to the non-valved RV-PA shunt remain controversial.

This study aimed to clarify the impact of diastolic regurgitation from PA to RV on ventricular energetics by conducting a theoretical analysis using computational models.

Methods

We modeled the cardiovascular systems of the Norwood procedure using the SPS, and valved and non-valved RV-PA shunts. The electrical analogs of the models used to simulate the cardiovascular systems are shown in Fig. 1. We modeled the postoperative cardiovascular systems mathematically by a combination of the time-varying elastance cardiac chamber model and the three-element Windkessel vascular model.

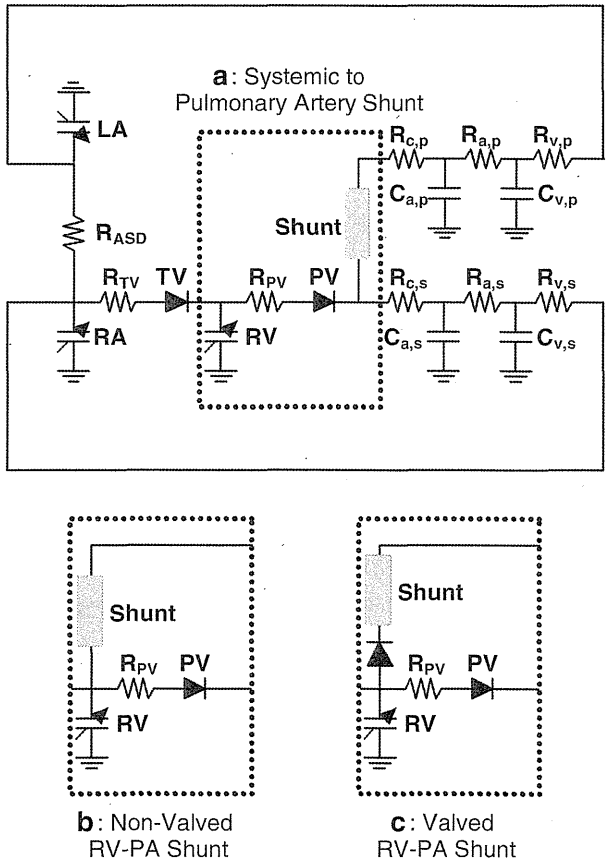

Fig. 1 Electrical analogs of Norwood procedures. **a** Norwood procedure with systemic to pulmonary shunt, **b** Norwood procedure with non-valved right ventricle to pulmonary artery (RV-PA) shunt, **c** Norwood procedure with valved RV-PA shunt. *LA* left atrium, *RA* right atrium, *RV* right ventricle, *PV* pulmonary valve, *TV* tricuspid valve, *ASD* atrial septal defect. R_a arterial resistance, R_c characteristic impedance, R_v venous resistance, C_a arterial capacitance, C_v venous capacitance. *s* and *p* systemic and pulmonary circulation, respectively. R_{PV}, R_{TV} and R_{ASD} resistance at PV, TV and ASD, respectively

Heart

The right ventricular and atrial chambers are represented by the time-varying elastance model [5–7]. The end-systolic pressure–volume relationship is described by a linear equation:

$$P_{es,cc} = E_{es,cc}[V_{es,cc} - V_{0,cc}] \quad (1)$$

where $P_{es,cc}$ is end-systolic pressure, $V_{es,cc}$ is end-systolic volume, $E_{es,cc}$ is the maximal volume elastance, $V_{0,cc}$ is the volume at which end-systolic pressure is equal to 0 mmHg, and cc denotes the right atrial (RA), left atrial (LA), or right ventricular (RV) chamber. The end-diastolic pressure–volume relationship is represented by a non-linear equation:

$$P_{ed,cc} = A_{cc}[e^{B_{cc}(V_{ed,cc}-V_{0,cc})} - 1] \quad (2)$$

where $P_{ed,cc}$ is end-diastolic pressure, $V_{ed,cc}$ is end-diastolic volume, A_{cc} and B_{cc} are constants [5–7]. We assumed the time course of elastance by defining normalized elastance curve $e_{cc}(t)$ as follows:

$$\begin{aligned} e_{cc}(t) &= 0.5\,[1 - \cos(\pi t/T_{es,cc})] \quad (0 \le t < 2T_{es,cc}) \\ e_{cc}(t) &= 0 \quad (2T_{es,cc} \le t < T_c) \end{aligned} \quad (3)$$

where t is the time from the start of systole, $T_{es,cc}$ is the time to the end of systole, and T_c is the duration of cardiac cycle. Using $e_{cc}(t)$, the instantaneous pressure–volume relationship is described by:

$$P_{cc}(t) = [P_{es,cc}(V_{cc}) - P_{ed,cc}(V_{cc})]e_{cc}(t) + P_{ed,cc}(V_{cc}) \quad (4)$$

Ventricular systole is preceded by atrial systole. The time advance of atrial systole (DT) is calculated as a fixed fraction of T_c (DT = 0.02 T_c) [9]. The function of each chamber is characterized by the parameters $E_{es,cc}$, $T_{es,cc}$, $V_{0,cc}$, A_{cc}, B_{cc} and $e_{cc}(t)$. The same $e_{cc}(t)$ is used for all chambers, but the other parameters are different between chambers, as shown in Table 1. Nonrestrictive atrial septal defect is described as constant resistance (R_{ASD}). Each valve is represented as an ideal diode connected serially to a small resistor (pulmonary R_{PV}, tricuspid R_{TV}).

Vascular system

Basically, the pulmonary and systemic circulations are modeled as modified Windkessel impedances. Each vascular system is modeled by lumped venous (C_v) and arterial (C_a) capacitances, a characteristic impedance (R_c) that is related to the stiffness of the proximal aorta or pulmonary artery, a lumped arterial resistance (R_a), and a

Table 1 Parameters used in modeling

Heart rate (HR) (beats/min)	160		
Duration of cardiac cycle (T_c) (ms)	375		
Time to end systole (T_{es}) (ms)	RV: 136	RA: 56	LA: 56
End-systolic elastance (E_{es}) (mmHg/ml)	RV: 8.5	RA: 7.35	LA: 7.35
Scaling factor of EDPVR (A) (mmHg)	RV: 0.9	RA: 0.17	LA: 0.17
Exponent for EDPVR (B) (ml^{-1})	RV: 0.062	RA: 0.484	LA: 0.484
Unstressed volume (V_0) (ml)	RV: 4	RA: 1	LA: 1
Valvular resistance (forward) (mmHg s ml^{-1})	Pulmonary: 0.0004	Tricupsid: 0.00004	
Resistance (mmHg s ml^{-1})	ASD: 0.001		
Index of pure viscous effects (k_1) [mmHg $(l/s)^{-1}$ mm^4]	Shunt: 5.76×10^4		
Index of convective acceleration (k_2) [mmHg $(l/s)^{-2}$ mm^4]	Shunt: 1.87×10^7		
Arterial resistance (R_a) (mmHg s ml^{-1})	Systemic (s): 3.83	Pulmonary (p): 0.63	
Characteristic impedance (R_c) (mmHg s ml^{-1})	Systemic (s): 0.20	Pulmonary (p): 0.028	
Venous resistance (R_v) (mmHg s ml^{-1})	Systemic (s): 0.083	Pulmonary (p): 0.011	
Arterial capacitance (C_a) (ml/mmHg)	Systemic (s): 0.50	Pulmonary (p): 0.31	
Venous capacitance (C_v) (ml/mmHg)	Systemic (s): 4.39	Pulmonary (p): 0.89	

RV right ventricle, *RA* right atrium, *LA* left atrium, *EDPVR* end-diastolic pressure–volume relation, *ASD* atrial septal defect

resistance proximal to C_v (R_v). This framework is similar to that used in deriving Guyton's resistance to venous return [8]. Arterial and venous capacitors for systemic circulation are denoted by $C_{a,s}$ and $C_{v,s}$, respectively, and those for pulmonary circulation by $C_{a,p}$ and $C_{v,p}$. The ratio of C_a to C_v is obtained from previous reports [6, 9, 10].

The relation between pressure (P_c) and volume (V_c) in each capacitance is described by the following linear equation:

$$P_c = \frac{V_c}{C} \tag{5}$$

The change in volume in each capacitance [$dV(t)/dt$] is described by the differential equation below:

$$\frac{dV(t)}{dt} = \sum Q_{inflow}(t) - \sum Q_{outflow}(t) \tag{6}$$

where $Q_{inflow}(t)$ and $Q_{outflow}(t)$ indicate the instantaneous volumetric flow rates at the inlet and outlet, respectively, of each compartment.

Pressure drop across the shunt

Flow of non-Newtonian fluid in a curved pipe is approximated as a quadratic function of $Q(t)$ [11, 12]. The instantaneous pressure drop across the shunt is described by:

$$\Delta P(t) = \frac{k_1 Q(t) + k_2 Q^2(t)}{D^4} \tag{7}$$

where $\Delta P(t)$ (mmHg) is pressure drop across the shunt, $Q(t)$ (l/s) is the instantaneous volume flow rate in shunt, D (mm) is the shunt diameter, k_1 [mmHg $(l/s)^{-1}$ mm^4] is the index of pure viscous effects and k_2 [mmHg $(l/s)^{-2}$ mm^4] is the index of convective acceleration [9].

Protocols

First, the control state was simulated using the 4.0-mm SPS model. Total stressed blood volume (V_s), which is the sum of the stressed volumes in all capacitances and in all chambers, was set as 80 ml.

$$V_s = V_{RV} + V_{LA} + V_{RA} + V_{C_{a,s}} + V_{C_{v,s}} + V_{C_{a,p}} + V_{C_{v,p}} \tag{8}$$

We solved the simultaneous differential equations (Eqs. 1–8) using MATLAB (MathWorks).

Shunt diameter (D) was decreased stepwise from 4.0 to 3.0 mm at decrements of 0.5 mm in the SPS model and increased from 4.0 to 6.0 mm at increments of 1.0 mm in both the valved and non-valved RV-PA shunt models. RV forward flow, systemic and pulmonary flows (Q_s and Q_p), systemic and pulmonary arterial pressures (SAP and PAP), right ventricular end-diastolic volume (RVEDV), stroke work (SW), systolic pressure–volume area (PVA) and mechanical efficiency after each procedure were calculated for each shunt diameter. Heart rate and mean SAP were set at the same values as those of the control state, by adjusting the total stressed blood volume (V_s).

Calculation of arterial and venous oxygen saturation

Since the total amount of O_2 present in the atrium is preserved and the decrease in O_2 content in blood balances the whole body O_2 consumption, arterial (SaO_2) and venous O_2 saturation (SvO_2) are calculated by the following equations for Q_p and Q_s (l/min):

$$SaO_2 = S_{PV}O_2 - \frac{CVO_2 \times BSA}{1.34 \times Hb \times 10 \times Q_p}$$

$$SvO_2 = SaO_2 - \frac{CVO_2 \times BSA}{1.34 \times Hb \times 10 \times Q_s}$$

where $S_{PV}O_2$ is the pulmonary venous O_2 saturation, CVO_2 (ml O_2/min/m^2) is the whole body O_2 consumption, BSA (m^2) is the body surface area, and Hb (g/dl) is the hemoglobin concentration. The constant 10 (dl/l) converts l to dl, and 1.34 (ml O_2/g) converts hemoglobin content to oxygen content. The following assumptions are used in the O_2 calculation: $S_{PV}O_2 = 0.97$ (dimensionless), $CVO_2 = 185$ ml O_2/min/m^2, BSA = 0.20 m^2 and Hb = 16.0 g/dl [9, 13].

Results

The hemodynamic parameters obtained from the computational simulations are shown in Table 2.

Although the increase in shunt diameter caused an increase in systolic SAP and a decrease in diastolic SAP in the SPS model, changes in shunt diameter only affect systolic and diastolic SAP slightly in both the valved and non-valved RV-PA shunt models. Despite the use of small caliber shunt in the SPS model, mean PAP, Q_p and Q_p/Q_s were higher than in both valved and non-valved RV-PA shunt models. Mean PAP, Q_p and Q_p/Q_s in the 3.5-mm SPS model were higher than those in the 6.0-mm non-valved RV-PA shunt model and almost equivalent to those in the 5.0-mm valved RV-PA shunt model.

Right ventricular pressure, SAP, PAP, aortic flow, and shunt flow in the 3.5-mm SPS, 6.0-mm non-valved shunt, and 5.0-mm valved RV-PA shunt models are shown in Fig. 2. In both valved and non-valved RV-PA shunt models, RV ejection to pulmonary circulation through the shunt preceded RV ejection to systemic circulation and continued even after the end of ejection to systemic circulation. Comparisons of the hemodynamics of the 3.5-mm SPS, and 5.0-mm valved and 6.0-mm non-valved RV-PA shunt models are shown in Fig. 3. RVEDV was smaller in the 6.0-mm non-valved RV-PA shunt (−3.7%) and the 5.0-mm valved RV-PA shunt (−11.7%) models than that in the 3.5-mm SPS model. At the same shunt diameter, mean PAP, Q_p, Q_p/Q_s, SaO_2 and SvO_2 were higher with the valved RV-PA shunt than with the non-valved shunt.

In the SPS model, the use of a larger conduit significantly increased systemic-to-pulmonary diastolic run-off and RVEDV (Table 2). In the valved and non-valved RV-PA shunt models, increase in conduit size likewise

Table 2 Hemodynamic data obtained from computational simulation of SPS, non-valved RV-PA shunt, and valved RV-PA shunt

	Mathematical models								
	SPS			Non-valved RV-PA			Valved RV-PA		
Shunt diameter (mm)	3.0	3.5	4.0	4.0	5.0	6.0	4.0	5.0	6.0
Heart rate (beats/min)	160			160			160		
Systolic systemic artery pressure (mmHg)	83.9	87.0	90.9	75.7	76.3	77.0	75.7	76.2	76.9
Diastolic systemic artery pressure (mmHg)	46.6	45.0	43.4	51.9	51.9	51.9	51.9	51.8	51.9
Mean systemic artery pressure (mmHg)	58.6	58.7	58.7	58.7	58.7	58.7	58.7	58.7	58.7
Mean PA pressure (mmHg)	10.4	13.8	17.3	7.50	9.83	11.9	8.98	12.6	16.2
RV forward flow (l/min)	1.60	1.86	2.14	1.53	1.86	2.19	1.51	1.81	2.10
Q_p (l/min)	0.77	1.04	1.32	0.55	0.73	0.90	0.68	0.98	1.27
Q_s (l/min)	0.83	0.82	0.82	0.83	0.83	0.83	0.83	0.83	0.83
Q_p/Q_s	0.94	1.26	1.62	0.66	0.88	1.09	0.81	1.18	1.54
Diastolic run-off (l/min)	0.52	0.69	0.85						
Diastolic regurgitation (l/min)				0.15	0.29	0.47			
SaO_2 (%)	74.7	80.4	83.9	65.4	73.5	77.8	71.5	79.3	83.4
SvO_2 (%)	53.9	59.5	62.8	44.8	52.8	56.9	50.8	58.5	62.5
Stressed blood volume (ml)	70.6	75.1	80.0	64.9	67.9	71.4	65.7	69.2	73.2
RVEDV (ml)	21.6	23.3	25.0	19.4	20.8	22.4	19.3	20.6	22.0
Stroke work (mmHg ml)	759	905	1,062	600	713	829	596	704	815
Systolic PVA (mmHg ml)	1,008	1,157	1,315	765	851	949	762	843	934
Mechanical efficiency (%)	75.3	78.2	80.8	78.4	83.8	87.4	78.3	83.5	87.2

SPS systemic to pulmonary artery shunt, *RV-PA* right ventricle to pulmonary artery shunt, *RV* right ventricle, *PA* pulmonary artery, Q_p pulmonary blood flow, Q_s systemic blood flow, SaO_2 arterial oxygen saturation, SvO_2 venous oxygen saturation, *RVEDV* right ventricular end-diastolic volume, *PVA* systolic pressure–volume area

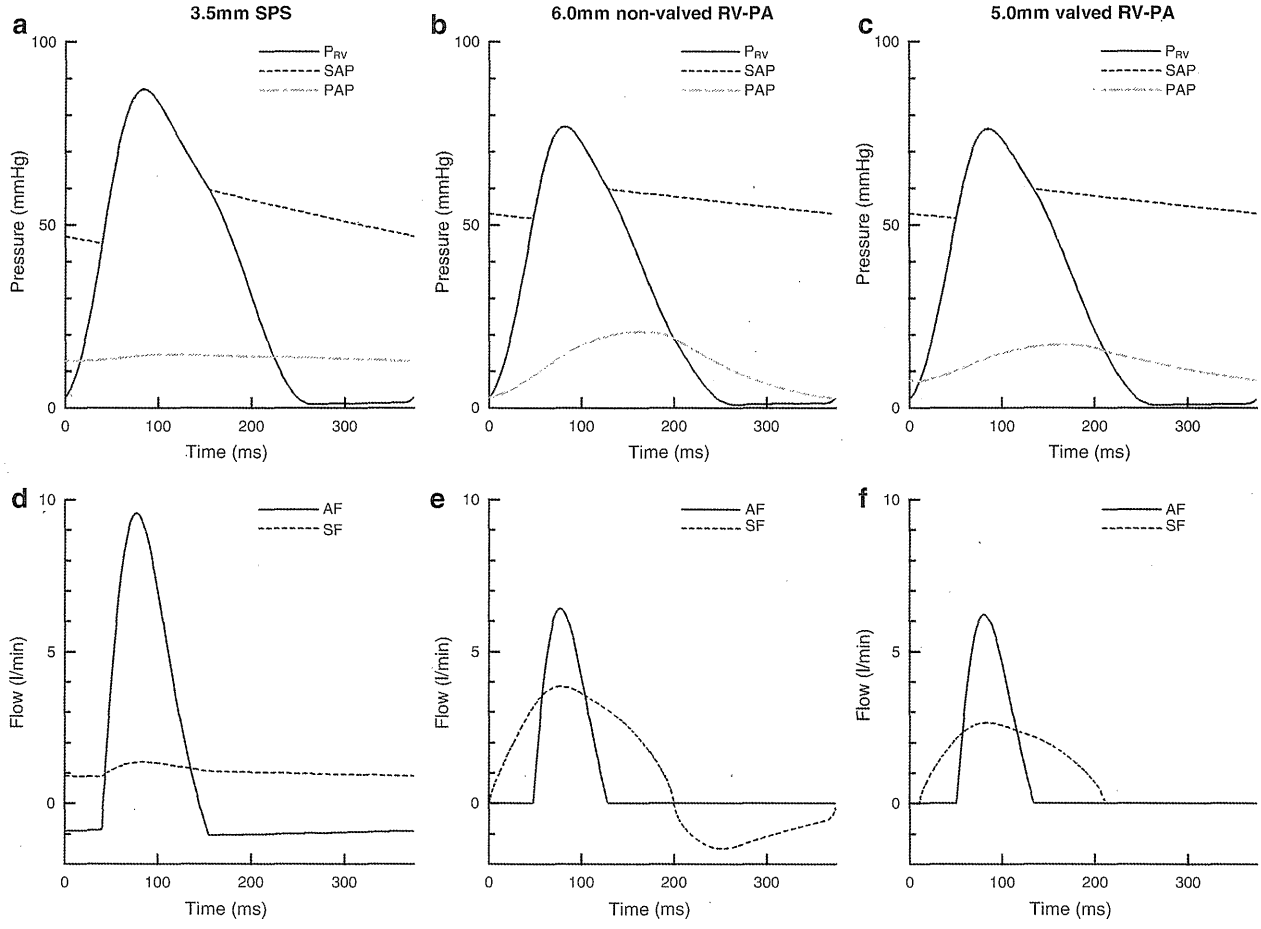

Fig. 2 Right ventricular pressure, systemic and pulmonary arterial pressures, aortic flow and shunt flow computed from the mathematical models of Norwood procedures with 3.5-mm systemic to pulmonary artery shunt (SPS **a**, **d**), 6.0-mm non-valved right ventricle to pulmonary artery (RV-PA) shunt (**b**, **e**), and 5.0-mm valved RV-PA shunt (**c**, **f**). P_{RV} right ventricular pressure, SAP systemic arterial pressure, PAP pulmonary arterial pressure, AF aortic flow, SF shunt flow

increased RVEDV, but the magnitudes were smaller than those of the SPS model, despite larger conduits being used in these models. The smaller RVEDV contributed to decreases in SW and PVA. The pressure–volume loops of the 3.5-mm SPS, and the 5.0-mm valved and 6.0-mm non-valved RV-PA shunt models are shown in Fig. 4. The SW in the 5.0-mm valved and 6.0-mm non-valved RV-PA shunts were −22.3 and −8.4%, respectively, smaller than that in the 3.5-mm SPS. The PVA in the 5.0-mm valved and 6.0-mm non-valved RV-PA shunts were −27.1 and −18.0%, respectively, smaller than that in the 3.5-mm SPS. Mechanical efficiency (SW/PVA) in the 5.0-mm valved and 6.0-mm non-valved RV-PA shunt were 5.3 and 9.2%, respectively, higher than that in the 3.5-mm SPS. Although the use of non-valved conduit caused diastolic regurgitation from PA to RV, there was no difference in mechanical efficiency between the valved and non-valved RV-PA shunts at the same shunt diameter. Furthermore, compared to the SPS and the valved RV-PA shunt, the non-valved RV-PA shunt delivered the highest mechanical efficiency at any given Q_p/Q_s (Fig. 5).

Discussion

The Norwood procedure for stage I palliation of the HLHS was first reported in 1983 [14]. In the conventional Norwood procedure, pulmonary circulation was maintained by a SPS, such as the modified Blalock–Taussig shunt. The development of the RV-PA shunt in the last decade has improved patient's mortality and morbidity [15]. Since Sano et al. [16] reported their experience with the non-valved RV-PA shunt in 2003, this modification has been widely used. However, it remains controversial whether the RV-PA shunt truly improves the outcome of the Norwood procedure.

The RV-PA shunt eliminates systemic to pulmonary diastolic run-off that occurs when using the SPS, which

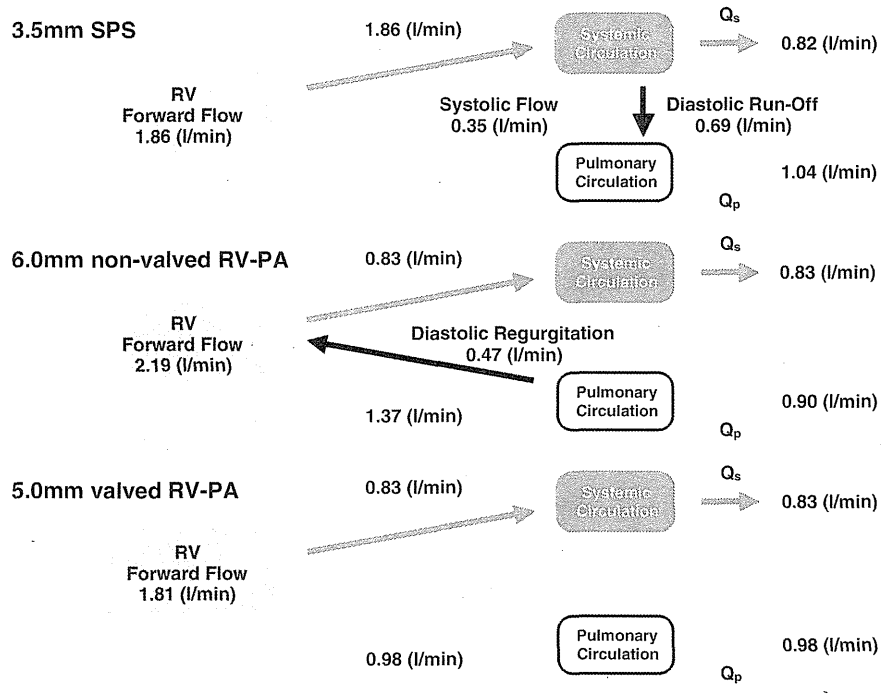

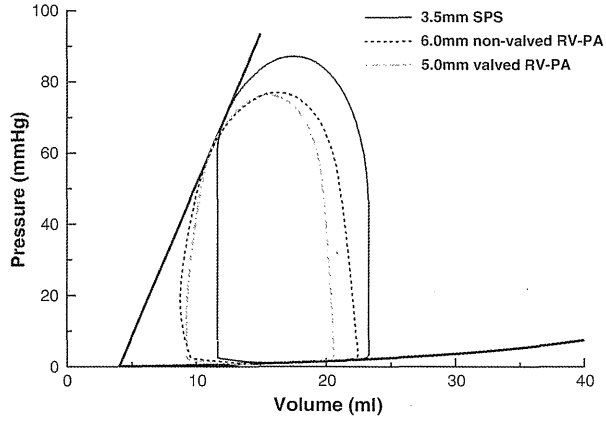

Fig. 4 Pressure-volume loops of simulated Norwood procedures. *Solid line* 3.5-mm systemic to pulmonary artery shunt (SPS), *dotted line* 6.0-mm non-valved right ventricle to pulmonary artery (RV-PA) shunt, *dot-dashed line* 5.0-mm valved RV-PA shunt

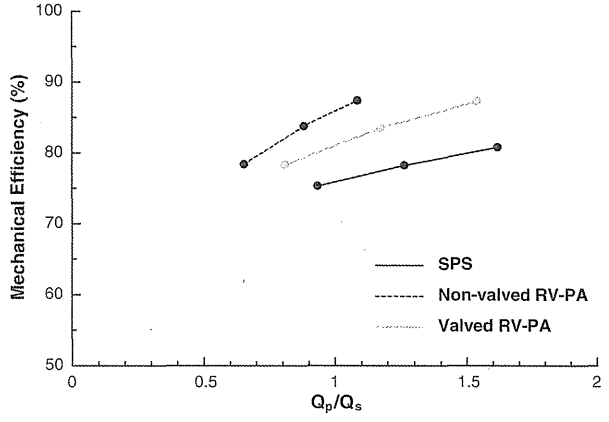

Fig. 5 The relation between Q_p/Q_s and mechanical efficiency. *Solid line* systemic to pulmonary artery shunt (SPS), *dotted line* non-valved right ventricle to pulmonary artery (RV-PA) shunt, *dot-dashed line* valved RV-PA shunt

causes a massive increase in ventricular preload. However, diastolic regurgitation from PA to RV is a drawback of the non-valved RV-PA shunt. Thus, some authors have reported the advantages of a valved RV-PA shunt [3, 4, 17]. Use of a valved RV-PA shunt prevents diastolic regurgitation from PA to RV, and should further decrease ventricular preload. However, the present theoretical study based on mathematical models revealed that the valved RV-PA shunt mainly improves pulmonary blood supply and the favorable effect on ventricular energetics is equivalent to that of the non-valved RV-PA shunt.

Influence on systemic circulation

In the SPS model, the use of a larger caliber shunt increased systolic SAP and decreased diastolic SAP. In both the valved and non-valved RV-PA shunt models, however, systolic and diastolic SAP did not change with the increase in shunt diameter. Diastolic SAP in both RV-PA shunt models were at most 8 mmHg higher than that in the SPS model. Some clinical reports have already demonstrated lower diastolic SAP using the SPS [18, 19]. Lower diastolic SAP may decrease coronary perfusion

pressure and result in coronary malperfusion. Therefore, excessive decrease in diastolic SAP when using the SPS may cause global myocardial ischemia and impair the postoperative surgical outcome. On the other hand, higher and stable diastolic SAP with both the valved and non-valved RV-PA shunts is favorable for myocardial blood supply.

Influence on pulmonary circulation

The Q_p was excessively high in the SPS model, but was lower in both the valved and non-valved RV-PA shunt models. The Q_p in the 3.5-mm SPS model was similar to that in the 5.0-mm valved RV-PA shunt and higher than that in the 6.0-mm non-valved RV-PA shunt model. The RV-PA shunts contributed to avoiding pulmonary over-circulation and maintaining appropriate pulmonary blood supply in spite of the larger conduits.

In the present study, the valved RV-PA shunt eliminated diastolic regurgitation from PA to RV, and improved pulmonary blood supply compared to the non-valved RV-PA shunt. At the same shunt diameter, Q_p was at most 42% higher in the valved RV-PA shunt than in the non-valved RV-PA shunt model. This resulted in higher oxygen saturation in the valved RV-PA shunt. To obtain the same Q_p as the valved RV-PA shunt, a non-valved RV-PA shunt may require larger stressed blood volume and may cause the increase in ventricular preload. Since some authors reported decreased SvO_2 as a predictor of morbidity after the Norwood procedure [20, 21], the valved RV-PA shunt that yields higher SvO_2 may be favorable for pulmonary circulation.

Caspi et al. [22] suggested that the Norwood procedure with RV-PA conduit may have favorable effects on the development of the pulmonary artery, which may be associated with the pulsatile pulmonary flow. The importance of pulsatility for the growth of pulmonary artery has been reported [23, 24]. The smaller pulsatility of pulmonary flow in the SPS as shown in Fig. 2d may impair the development of the pulmonary artery.

Influence on RVEDV

The RVEDV was markedly reduced in both the non-valved and valved RV-PA shunt models compared to the SPS model. When using a SPS, systemic and pulmonary arteries are directly connected. Therefore, a blood shift from systemic to pulmonary circulation in the diastolic phase (diastolic run-off) cannot be avoided, because pulmonary vascular resistance is usually lower than systemic vascular resistance. This should cause a decrease in systemic arterial pressure and require a greater stressed blood volume to maintain the mean SAP (Table 2), resulting in increased RVEDV and Q_p. When the RV-PA shunts are used, since systemic and pulmonary arteries originate separately from the RV, diastolic run-off is avoided and RVEDV and Q_p are lower as a result. The lower RVEDV contributes to improvement of ventricular energetics as described below.

Influence on ventricular energetics

Diastolic regurgitation from PA to RV occurs when a non-valved RV-PA shunt is used. It is possible that the diastolic regurgitation may increase ventricular preload and impair ventricular energetics compared to the valved RV-PA shunt. However, the present study demonstrated that use of both the valved and non-valved RV-PA shunts eliminated systemic to pulmonary diastolic run-off and improved mechanical efficiency (SW/PVA) to the same extent. Compared to the 3.5-mm SPS model, the lower RVEDV in both the 5.0-mm valved and 6.0 mm non-valved RV-PA shunt models contributed to decreasing PVA (−27.2 and −18.0%, respectively) and increasing mechanical efficiency (+5.3 and +9.2%, respectively). Therefore, the influence of diastolic regurgitation associated with the non-valved RV-PA shunt may be small from the viewpoint of ventricular energetics. Because PVA correlates significantly with myocardial oxygen consumption [24], decreased PVA results in reduced myocardial oxygen demand. The present results suggest that both RV-PA shunts reduce myocardial oxygen demand.

This advantage of both RV-PA shunts in ventricular energetics may be associated with the RV ejection pattern through the RV-PA shunts. With the SPS, RV has to pump the blood to a higher pressure system i.e., the systemic circulation. This limits the duration of RV ejection and requires higher RV systolic pressure. However, with both the RV-PA shunts, the systemic and pulmonary arteries originate separately from the RV. The RV ejects blood steadily via the RV-PA shunt to the pulmonary circulation that has a relatively low pressure (Fig. 2). This fact may contribute to the decreased SW and PVA when using the valved and non-valved RV-PA shunts.

Advantage of RV-PA shunt

The higher diastolic SAP obtained from using a RV-PA shunt has been reported to improve coronary blood supply [1]. However, under physiological conditions, coronary blood flow depends on myocardial oxygen demand [25]. The greatest advantage of the RV-PA shunt is that this procedure decreases myocardial oxygen demand through decreasing PVA. The RV-PA shunt is able to maintain systemic circulation at lower oxygen consumption compared to the SPS, implying that the RV-PA shunt requires less coronary blood flow than the SPS to maintain the same

Table 3 The influence of ventriculotomy on ventricular energetics

	$E_{es,RV}$ (mmHg/ml)	SW (mmHg ml)	PVA (mmHg ml)	Mechanical efficiency (%)
3.5-mm SPS	8.5	905	1,157	78.2
6.0-mm non-valved RV-PA	7.5	827	977	84.7
	6.5	825	1,018	81.1
5.0-mm valved RV-PA	7.5	702	875	80.3
	6.5	698	916	76.2

SPS systemic to pulmonary artery shunt, *RV-PA* right ventricle to pulmonary artery shunt, $E_{es,RV}$ end-systolic elastance of right ventricle, *SW* stroke work, *PVA* systolic pressure–volume area

systemic circulation. This feature may contribute to the improvement of coronary flow reserve. The RV-PA shunt may have better tolerance to the postoperative myocardial ischemia.

Limitations

The present study had some limitations. First, the potential damage of right ventriculotomy was disregarded in the present simulations. Ventricular incision is required to place the valved or non-valved RV-PA shunt. Although ventriculotomy may cause ventricular systolic dysfunction or tricuspid regurgitation, Graham et al. [26] observed no apparent deleterious effects of right ventriculotomy following the Norwood procedure using a RV-PA shunt. Furthermore, our additional simulation suggested that the RV-PA shunt still improved ventricular energetics in spite of the potential damage of ventriculotomy, which decreased the end-systolic elastance of RV ($E_{es,RV}$) from 8.5 to 7.5 mmHg/ml (Table 3). However, mechanical efficiency in the 5.0-mm valved RV-PA shunt would be lower than that in the 3.5-mm SPS when ventriculotomy decreased $E_{es,RV}$ to 6.5 mmHg/ml.

Second, systemic and pulmonary vascular resistance did not change in the present simulations. Vascular resistance was the same in all three shunt models. The differences in pulsatility of the three procedures may affect vascular resistance. A previous report indicated that a sudden increase in systemic vascular resistance caused circulatory collapse in Norwood patients [27]. Therefore, further analyses on the influence of vascular resistance are required.

Third, inertial effects in the shunt were disregarded in the present study. If we considered flow in the shunt as unsteady flow, inertial effects would have a great impact on the pressure-drop across the shunt. [28] Then, the length of shunt might become a strong determinant of pressure–flow relationship.

Conclusions

The present theoretical analysis indicates that both the valved and non-valved RV-PA shunts maintain adequate pulmonary circulation; as a result, the RV delivers greater SW for a lower PVA, i.e., lower myocardial oxygen consumption. Although the valved RV-PA shunt improves pulmonary blood supply and consequently increases Q_p and oxygen saturation compared to the non-valved RV-PA shunt, the favorable effects of the two RV-PA shunts on ventricular energetics are equivalent. The non-valved RV-PA shunt reduces PVA and improves mechanical efficiency in spite of the presence of PA to RV regurgitation.

Acknowledgments This study was supported by a research project promoted by the Japanese Ministry of Health, Labour and Welfare (H20-katsudo-Shitei-007 and H21-nano-Ippan-005); Grants-in-Aid for Scientific Research (No. 20390462, No. 22791328 and No. 23390415) from the Ministry of Education, Culture, Sports, Science and Technology; and the Industrial Technology Research Grant Program from New Energy and Industrial Technology Development Organization (NEDO) of Japan.

References

1. Maher KO, Pizarro C, Gidding SS, Januszewska K, Malec E, Norwood WI Jr, Murphy JD (2003) Hemodynamic profile after the Norwood procedure with right ventricle to pulmonary artery conduit. Circulation 108:782–784
2. Bove EL, Migliavacca F, de Leval MR, Balossino R, Pennati G, Lloyd TR, Khambadkone S, Hsia TY, Dubini G (2008) Use of mathematic modeling to compare and predict hemodynamic effects of the modified Blalock–Taussig and right ventricle-pulmonary artery shunts for hypoplastic left heart syndrome. J Thorac Cardiovasc Surg 136:312–320.e2
3. Reinhartz O, Reddy VM, Petrossian E, MacDonald M, Lamberti JJ, Roth SJ, Wright GE, Perry SB, Suleman S, Hanley FL (2006) Homograft valved right ventricle to pulmonary artery conduit as a modification of the Norwood procedure. Circulation 114:I594–I599
4. Takeuchi K, Murakami A, Takaoka T, Takamoto S (2006) Evaluation of valved saphenous vein homograft as right ventricle-pulmonary artery conduit in modified stage I Norwood operation. Interact Cardiovasc Thorac Surg 5:345–348
5. Burkhoff D, Tyberg JV (1993) Why does pulmonary venous pressure rise after onset of LV dysfunction: a theoretical analysis. Am J Physiol 265:H1819–H1828
6. Morley D, Litwak K, Ferber P, Spence P, Dowling R, Meyns B, Griffith B, Burkhoff D (2007) Hemodynamic effects of partial ventricular support in chronic heart failure: results of simulation validated with in vivo data. J Thorac Cardiovasc Surg 133:21–28
7. Shimizu S, Shishido T, Une D, Kamiya A, Kawada T, Sano S, Sugimachi M (2010) Right ventricular stiffness constant as a predictor of postoperative hemodynamics in patients with

hypoplastic right ventricle: a theoretical analysis. J Physiol Sci 60:205–212
8. Sagawa K, Maughan L, Suga H, Sunagawa K (1988) Cardiovascular interaction. In: Sagawa K, Maughan L, Suga H, Sunagawa K (eds) Cardiac contraction and the pressure–volume relationship. Oxford University Press, Oxford
9. Migliavacca F, Pennati G, Dubini G, Fumero R, Pietrabissa R, Urcelay G, Bove EL, Hsia TY, de Leval MR (2001) Modeling of the Norwood circulation: effects of shunt size, vascular resistances, and heart rate. Am J Physiol Heart Circ Physiol 280:H2076–H2086
10. Huikeshoven F, Coleman TG, Jongsma HW (1980) Mathematical model of the fetal cardiovascular system: the uncontrolled case. Am J Physiol 239:R317–R325
11. Migliavacca F, Dubini G, Pennati G, Pietrabissa R, Fumero R, Hsia TY, de Leval MR (2000) Computational model of the fluid dynamics in systemic-to-pulmonary shunts. J Biomech 33:549–557
12. Young DF, Tsai FY (1973) Flow characteristics in models of arterial stenoses. I. Steady flow. J Biomech 6:395–410
13. Chang AC, Kulik TJ, Hickey PR, Wessel DL (1993) Real-time gas-exchange measurement of oxygen consumption in neonates and infants after cardiac surgery. Crit Care Med 21:1369–1375
14. Norwood WI, Lang P, Hansen DD (1983) Physiologic repair of aortic atresia-hypoplastic left heart syndrome. N Engl J Med 308:23–26
15. Pizarro C, Malec E, Maher KO, Januszewska K, Gidding SS, Murdison KA, Baffa JM, Norwood WI (2003) Right ventricle to pulmonary artery conduit improves outcome after stage I Norwood for hypoplastic left heart syndrome. Circulation 108:II155–II160
16. Sano S, Ishino K, Kawada M, Arai S, Kasahara S, Asai T, Masuda Z, Takeuchi M, Ohtsuki S (2003) Right ventricle-pulmonary artery shunt in first-stage palliation of hypoplastic left heart syndrome. J Thorac Cardiovasc Surg 126:504–509
17. Yamashiro M, Morita K, Uno Y, Shinohara G, Hashimoto K (2011) Modified Norwood procedure with a handmade downsizing valved right ventricle-to-pulmonary artery conduit. Gen Thorac Cardiovasc Surg 59:30–33
18. Bradley SM, Simsic JM, McQuinn TC, Habib DM, Shirali GS, Atz AM (2004) Hemodynamic status after the Norwood procedure: a comparison of right ventricle-to-pulmonary artery connection versus modified Blalock–Taussig shunt. Ann Thorac Surg 78:933–941
19. Azakie A, Martinez D, Sapru A, Fineman J, Teitel D, Karl TR (2004) Impact of right ventricle to pulmonary artery conduit on outcome of the modified Norwood procedure. Ann Thorac Surg 77:1727–1733
20. Hoffman GM, Ghanayem NS, Kampine JM, Berger S, Mussatto KA, Litwin SB, Tweddell JS (2000) Venous saturation and the anaerobic threshold in neonates after the Norwood procedure for hypoplastic left heart syndrome. Ann Thorac Surg 70:1515–1520
21. Hoffman GM, Tweddell JS, Ghanayem NS, Mussatto KA, Stuth EA, Jaquis RD, Berger S (2004) Alteration of the critical arteriovenous oxygen saturation relationship by sustained afterload reduction after the Norwood procedure. J Thorac Cardiovasc Surg 127:738–745
22. Caspi J, Pettitt TW, Mulder T, Stopa A (2008) Development of the pulmonary arteries after the Norwood procedure: comparison between Blalock–Taussig shunt and right ventricular-pulmonary artery conduit. Ann Thorac Surg 86:1299–1304
23. Malec E, Januszewska K, Kolcz J, Mroczek T (2003) Right ventricle-to-pulmonary artery shunt versus modified Blalock–Taussig shunt in the Norwood procedure for hypoplastic left heart syndrome—influence on early and late haemodynamic status. Eur J Cardiothorac Surg 23:728–733
24. Suga H, Yasumura Y, Nozawa T, Futaki S, Igarashi Y, Goto Y (1987) Prospective prediction of O_2 consumption from pressure-volume area in dog hearts. Am J Physiol 252:H1258–H1264
25. Tune JD, Gorman MW, Feigl EO (2004) Matching coronary blood flow to myocardial oxygen consumption. J Appl Physiol 97:404–415
26. Graham EM, Atz AM, Bradley SM, Scheurer MA, Bandisode VM, Laudito A, Shirali GS (2007) Does a ventriculotomy have deleterious effects following palliation in the Norwood procedure using a shunt placed from the right ventricle to the pulmonary arteries? Cardiol Young 17:145–150
27. Wright GE, Crowley DC, Charpie JR, Ohye RG, Bove EL, Kulik TJ (2004) High systemic vascular resistance and sudden cardiovascular collapse in recovering Norwood patients. Ann Thorac Surg 77:48–52
28. Young DF, Tsai FY (1973) Flow characteristics in models of arterial stenoses. II. Unsteady flow. J Biomech 6:547–559

Gen Thorac Cardiovasc Surg (2011) 59:672–680
DOI 10.1007/s11748-010-0685-9

ORIGINAL ARTICLE

Impact of chronic cyanosis and reoxygenation on the microheterogeneity of the myocardial blood flow: digital radiographic study in neonatal rats

Tomoko Tomii, MD · Osami Honjo, MD, PhD
Takeshi Matsumoto, PhD · Hiroyuki Tachibana, PhD
Yasuhiro Fujii, MD, PhD · Kozo Ishino, MD, PhD
Yasuo Ogasawara, PhD · Shunji Sano, MD, PhD

Received: 4 February 2010 / Accepted: 20 July 2010

Abstract
Purpose. This study sought to show the heterogeneity of myocardial blood flow in the chronically hypoxic infantile myocardium and its response to reoxygenation using a novel type of digital radiography.
Methods. Newborn rats were housed in a hypoxic chamber or in a normal chamber (controls). After 4 or 8 weeks, the control rats were ventilated with normoxic conditions, and the rats housed under hypoxia were ventilated with either hypoxic (cyanotic group) or normoxic conditions (reoxygenation group). Desmethylimipramine labeled with tritium (HDMI) was injected into the left ventricle, and both ventricular free walls were sectioned and sliced from the subepicardium to the subendocardium at 10 mm thickness. The within-layer distribution of HDMI density was measured by digital radiography, and its spatial heterogeneity (i.e., flow heterogeneity) was quantified by the coefficient of variation (CV) of flows.
Results. There were no differences in the CV between the groups in either ventricle at 4 weeks of age and no differences in the right ventricle at 8 weeks of age. There was a trend toward a higher left ventricular CV in the cyanotic group than in the control group at 8 weeks of age (0.637 ± 0.099 vs. 0.510 ± 0.060, $P = 0.06$). At 8 weeks of age, the CV was lower in both ventricles in the reoxygenation group than in those of the control and cyanotic groups.
Conclusion. The chronically hypoxic infantile myocardium exhibits regional flow heterogeneity similar to that observed in the normal myocardium in both ventricles and exhibits reduced flow heterogeneity in response to reoxygenation.

Key words Cyanotic heart · Microheterogeneity · Digital radiography · Myocardial blood flow

T. Tomii · Y. Fujii · S. Sano
Department of Cardiovascular Surgery, Okayama University Graduate School of Medicine and Dentistry, Okayama, Japan

O. Honjo (✉)
Division of Cardiovascular Surgery, The Hospital for Sick Children, The University of Toronto, 555 University Avenue, Toronto, ON, M5G 1X8, Canada
Tel. +1-416-813-6420; Fax +1-416-813-7984
e-mail: osami47@hotmail.com

O. Honjo
The Labatt Family Heart Centre, The Hospital for Sick Children, The University of Toronto, Toronto, Canada

T. Matsumoto
Department of Mechanical Science and Bioengineering, Osaka University Graduate School of Engineering Science, Toyonaka, Japan

H. Tachibana
Department of Medical Engineering, Faculty of Health Science and Technology, Kawasaki University of Medical Welfare, Kurashiki, Japan

K. Ishino
Circulatory Center, Showa University Northern Yokohama Hospital, Yokohama, Japan

Y. Ogasawara
Department of Medical Engineering and Systems Cardiology, Kawasaki Medical School, Kurashiki, Japan

Introduction

Regional myocardial blood flow shows considerable spatial heterogeneity (region-to-region flow variability) even in the normal state.[1,2] Here, "region-to-region flow variability"

means the difference between flows in small regions within myocardial layers (i.e., flow heterogeneity at the lowest level). Myocardial spatial flow heterogeneity is stable,[3] and its physiological significance is linked with the efficiency of the O_2 supply in the tissue. The determinants of the heterogeneity of regional myocardial flow are coronary vascular tone, coronary anatomy, and cardiac mechanical effects on coronary flow, in which vascular tone is essential.[4] Even at rest in the normal heart, the spatial flow heterogeneity is under the strong influence of vascular tone so regional O_2 supplies match well with myocardial O_2 requirements in those corresponding regions.

Owing to inherently high O_2 extraction in the myocardium, flow heterogeneity is highly sensitive to insufficient O_2 supply. That is, compensatory vasodilation in response to reduced O_2 supply increases regional flow and, accordingly, changes the spatial flow heterogeneity. Regional myocardial flow may be regulated to be less heterogeneous under acute hypoxia. Matsumoto et al. showed hypoxia-induced reduction of within-layer flow heterogeneity in rabbit hearts by digital radiography with 100-μm pixel resolution.[5] Focusing on the differences in regional myocardial O_2 extraction,[6] the same authors speculated that flow in originally low-flow regions increase to a higher degree under hypoxia because of relatively higher O_2 extraction in those low-flow regions. On the other hand, Austin et al. reported that regional myocardial flow is more heterogeneous under asphyxia or the maximally vasodilatory condition induced by adenosine administration than under normoxia, although the tissue size resolved (several hundred millimeters) is much larger than 100 μm.[4,7] The mechanism underlying the O_2 dependence of myocardial flow heterogeneity remains to be clarified.

Myocardium in infants with cyanotic congenital heart disease is exposed to chronic hypoxia, resulting from severe pulmonary stenosis or atresia, or a right-to-left shunt. A chronically hypoxic myocardium in patients with tetralogy of Fallot has depressed adenosine triphosphate (ATP), defects in oxidative metabolism, and subsequent depressed postoperative ventricular function.[8] In contrast, a substantial body of evidence shows that the chronically hypoxic myocardium is preconditioned to ischemic events, thereby protecting against severe ischemic insult.[9] These studies suggest that the physiological response of the chronically hypoxic myocardium to ischemia or reperfusion (reoxygenation) is different from that of the normal myocardium. The following hypotheses were examined in this study: (1) chronically hypoxic myocardium differs (in terms of vascular tone or local vascular regulation) from the normal myocardium, thereby differing from the normal myocardium in terms of myocardial flow heterogeneity; (2) the coronary vasoresponse to reoxygenation of chronically hypoxic myocardium differs from that of normal myocardium, thereby affecting the flow heterogeneity under reoxygenation of the chronically hypoxic myocardium differently from that of normal myocardium.

Digital radiography combined with the technique of tritium-labeled desmethylimipramine (HDMI), an α-adrenergic antagonist, deposition for assessing regional myocardial flow was used to test these hypotheses. This technique enables the assessment of myocardial flow distribution with a resolution of 100 mm, which is ideal for evaluating myocardial flow at a precapillary level.[5] The chronic hypoxic model was developed by housing neonatal rats under a hypoxic environment for 4 and 8 weeks, thereby mimicking tetralogy of Fallot or other cyanotic congenital heart disease undergoing intracardiac repair and reoxygenation as in humans during infancy or childhood.[10]

Materials and methods

The experimental protocol was approved by the Committee on Animal Research at Okayama University, Japan. The animals were treated in compliance with the Principles of Laboratory Animal Care established by the National Society for Medical Research and the Guide for the Care and Use of Laboratory Animals established by the Institute of Laboratory Animal Resources and published by the National Institute of Health (NIH publication 86-23, revised 1985).

Animal preparation

Sprague-Dawley pregnant female rats were housed in ambient air. Within 24 h after delivery, the neonatal rats and their mother rat were moved into a hypoxic chamber (cyanotic group) or a normal cage under ambient air (controls) and housed together during the lactation period. Thereafter, the neonatal rats were housed alone until the age of 4 or 8 weeks. O_2 and CO_2 concentrations in the hypoxic chamber were maintained at 12%–14% and <0.4%, respectively, using a custom-made hypo-O_2 producing device (Teijin, Tokyo, Japan). The gas concentrations were continuously monitored using a gas analyzer (ML206; AD Instruments, Sydney, Australia) and recorded by commercially available software (PowerLab; AD Instruments). Humidity was maintained at <75% and the temperature at 23°–27°C. These concentrations were monitored with a hygrothermometer (TRH-7X; Shinyei, Kobe, Japan). The animals were kept under a 12:12-h light–dark cycle; and standard rat chow and tap water were provided ad libitum.

Digital radiographic study

Preparation and ventilation

After 4 or 8 weeks of chronic hypoxia, animals were placed in the ambient environment and anesthetized with pentobarbital sodium (30 mg/kg i.p.). Body temperature was maintained at 37°–38°C on a heating blanket. After endotracheal intubation through a tracheotomy, each animal was artificially ventilated with a tidal volume of 10 ml/kg and a frequency of 55–65 strokes/min. The rats in the Control group ($n = 6$ and 7 at the ages of 4 and 8 weeks, respectively) were ventilated normally with a fraction of inspired O_2 (FiO_2) of 0.34–0.38. Electrocardiograms were continuously recorded on a direct-writing system (model RM6200; Nihon Kohden, Tokyo, Japan). A femoral vein was cannulated for drug infusion and blood sampling. A carotid or femoral artery was cannulated for arterial blood gas measurement. The heart was exposed by a median sternotomy. Arterial partial pressures of O_2 (PO_2) and CO_2 (PCO_2) and the pH were adjusted to be within physiological limits. The rats in the Cyanotic group ($n = 6$ each at the ages of 4 and 8 weeks) were ventilated with a "hypoxic" setting where FiO_2 and CO_2 fractions were 0.12–0.14 and <0.01, respectively. In the third group (reoxygenation group), the cyanotic animals ($n = 6$ each at the ages of 4 and 8 weeks, respectively) were subjected to "normal" ventilation in the same manner as in the control group.

Sample preparation

After the hemodynamics were stabilized and the ventilatory setting was adjusted based on the blood gas analysis, 20 μCi of desmethylimipramine labeled with tritium (HDMI), molecular weight 302.8 (no. NET 593; Du Pont-New England Nuclear, Waltham, MA, USA) was injected into the left ventricle (LV) through the apex using a 0.1-ml glass syringe over a period of 4–5 s. One minute after the injection of HDMI, the heart was arrested with an intravenous injection of a saturated potassium chloride solution and harvested en bloc. In the reoxygenation group, it took about 40 min from the start of reoxygenation to harvest. After the blood was washed out by saline, the free walls of the LV and the right ventricle (RV) were excised. The samples were sandwiched in aluminum sheets without compression and immediately placed in a −80°C freezer. The frozen sample was then sliced into more than 20 slices at 10 μm thickness from the subepicardium to the subendocardium by a cryostat microtome (HM505EVA; Zeiss, Hennigsdorf, Germany). Each slice was then placed on a slide glass and dried overnight.

Digital radiographic analysis

The digital radiographic technique is described in detail elsewhere.[5,11] Briefly, the slices were exposed to an imaging plate (IP-TR2040; Fujix, Kyoto, Japan), a two-dimensional sensor of tritium-sensitive radioactive energy, for 3 days in a lead-shielded box. The distribution of regional tissue radioactivity recorded on the imaging plate was converted to 16-bit digital data with 100-μm pixels by Bio-imaging analyzer (model HGE; Fujix), and the relative flow distribution was visualized with a 66536-step gradation. The mean background density was <5% of that of a region overlying the tissue.

For the analysis of within-layer flow distribution, 6–10 digital radiograms were arbitrarily selected from the subepicardium and the subendocardium of LV and RV free walls. Epicardial layer images showing a large coronary vessel trace were excluded from the study. Corrected for background activity, the heterogeneity of within-layer flows was quantitated by calculating the coefficient of pixel-to-pixel flow variation (CV; standard deviation/mean) in a square portion (3 × 3 mm to 6 × 6 mm) of each image. Figure 1 shows typical examples of within-layer flow distribution in the LV for three groups. The shading of the images is proportional to regional flow.

Morphometric and hemodynamic measurements

The body weight; weights of the whole heart (WH), RV, and LV; the thicknesses of the RV and LV free walls, and the hematocrit were measured. In another set of 8-week-old cyanotic ($n = 10$) and normal ($n = 7$) rats, the arterial blood pressure and heart rate were measured before and after sternotomy. The changes in the blood pressure and heart rate from hypoxic to normal ventilation were also recorded in the cyanotic rats. The blood pressure was measured using a pressure transducer (model 420-4; Camino Labs) and a manometer catheter (model 110-4 Fr; Camino Labs, San Diego, CA, USA) that had been inserted into the internal carotid artery.

Statistical methods

The data are presented as the mean ± SD. The level of statistical significance was set at $P < 0.05$. Differences among the three groups were analyzed by an analysis of variance (ANOVA) followed by post-hoc tests. Differences between groups were assessed by F-test followed by an unpaired *t*-test or the Mann-Whitney U-test. The CV was assessed by the Mann-Whitney U-test.

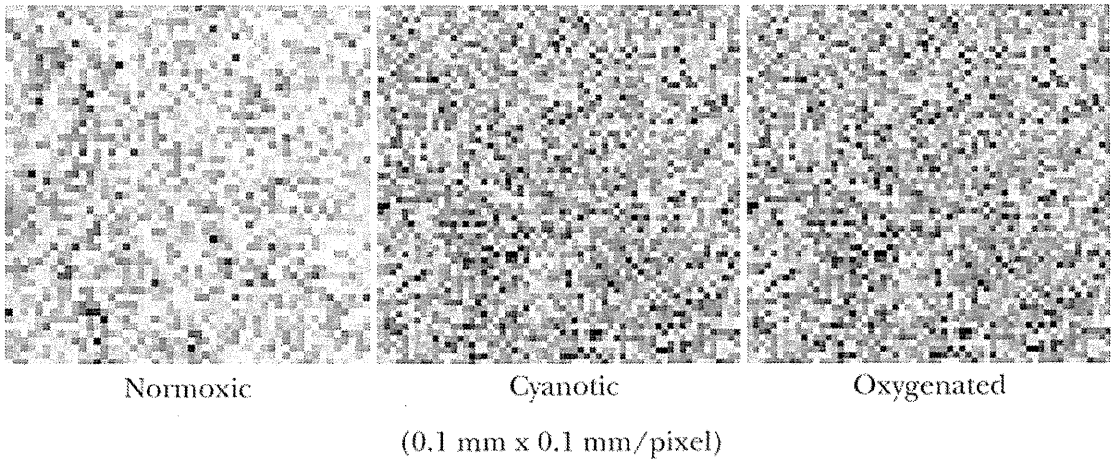

Fig. 1 Typical examples of desmethylimipramine labeled with tritium (HDMI) tracer images showing within-layer flow distributions in the left ventricular (LV) myocardium in control, cyanotic, and reoxygenated heart tissue

Table 1 Body and heart weights and ventricular wall thickness in normal and cyanotic myocardium

Parameter	4 Weeks			8 Weeks		
	Cyanotic ($n = 15$)	Control ($n = 7$)	P	Cyanotic ($n = 12$)	Control ($n = 8$)	P
Body weight (g)	75 ± 25	138 ± 30	<0.0001	166 ± 33	324 ± 17	<0.0001
Whole heart (g)	0.48 ± 0.16	0.66 ± 0.15	<0.05	0.84 ± 0.21	1.08 ± 0.12	<0.05
WH/BW × 10^{-2}	0.66 ± 0.19	0.49 ± 0.11	<0.05	0.50 ± 0.12	0.34 ± 0.04	<0.01
LV weight (g)	0.27 ± 0.11	0.37 ± 0.13	0.07	0.47 ± 0.14	0.60 ± 0.13	<0.05
LV weight/WH	0.56 ± 0.12	0.56 ± 0.14	0.97	0.55 ± 0.07	0.56 ± 0.11	0.95
RV weight (g)	0.12 ± 0.06	0.10 ± 0.04	0.38	0.18 ± 0.06	0.18 ± 0.06	0.96
RV weight/WH	0.25 ± 0.07	0.15 ± 0.07	<0.05	0.22 ± 0.04	0.17 ± 0.04	<0.05
RV/LV ratio	0.45 ± 0.13	0.27 ± 0.10	<0.01	0.40 ± 0.11	0.31 ± 0.12	0.10
Hematocrit (%)	46 ± 6	43 ± 3	0.21	56 ± 7	45 ± 5	<0.001
LV thickness (mm)	2.61 ± 0.54	2.57 ± 0.60	0.90	2.65 ± 1.15	4.21 ± 1.32	<0.05
RV thickness (mm)	1.66 ± 0.46	1.49 ± 0.58	0.48	2.52 ± 0.96	1.38 ± 0.18	<0.05

WH, whole heart; BW, body weight; LV, left ventricle; RV, right ventricle

Results

Characteristics of the cyanotic rat model

The body weights were significantly lower in the 4- and 8-week-old cyanotic rats in comparison to those in age-matched control rats ($P < 0.0001$) (Table 1). Cyanotic rat hearts show RV hypertrophy characterized by a higher WH-to-body weight ratio (WH/BW) and higher RV/WH ratio at both ages, and a higher RV/LV ratio at 4 weeks of age, in comparison to those in the age-matched control rats ($P < 0.05$ for all), although there was no difference in RV weight between the age-matched groups (Table 1). A higher hematocrit was found in the 8-week-old cyanotic rats than in the age-matched control rats ($P < 0.001$). The LV and RV wall thicknesses did not differ between the groups at 4 weeks of age. Smaller LV wall thickness and larger RV wall thickness were found in the 8-week-old cyanotic rats in comparison to those in the age-matched control rats ($P < 0.05$ for both).

Cyanotic versus control rats

Blood gases and hemodynamics are shown in Table 2. Arterial PaO_2 and saturation (SaO_2) were significantly lower in the cyanotic group than those in the control group. Cyanotic rats at 4 weeks of age were acidotic, characterized by lower pH and bicarbonate, in comparison to those in the age-matched control rats ($P < 0.01$). There was no difference in heart rate between the groups at either age. At 8 weeks of age, no sternotomy-induced change was found in the blood pressure or heart rate in both groups.

Table 2 Hemodynamic and metabolic parameters in normal, hypoxic, and reoxygenated myocardium

Parameter	4 Weeks				8 Weeks			
	Cyanotic ($n = 8$)	Oxygenated ($n = 7$)	Normal ($n = 7$)	P	Cyanotic ($n = 6$)	Oxygenated ($n = 6$)	Normal ($n = 8$)	P
HR (bpm)	349 ± 90	372 ± 28	421 ± 83	0.19	412 ± 76	383 ± 56	366 ± 23	0.30
pH	7.23 ± 0.09*	7.32 ± 0.04*	7.42 ± 006	<0.001	7.36 ± 0.04	7.43 ± 0.03	7.41 ± 0.05	<0.05
PaO_2 (mmHg)	50 ± 9*	162 ± 33	174 ± 39	<0.0001	43 ± 7*	192 ± 18	191 ± 39	<0.0001
$PaCO_2$ (mmHg)	33 ± 6	39 ± 9	35 ± 7	0.24	40 ± 3	37 ± 3	39 ± 5	0.46
HCO_3 (mmol/l)	14 ± 4*	20 ± 4	22 ± 4	<0.01	23 ± 1	25 ± 2	24 ± 2	0.31
SaO_2 (%)	77 ± 5*	99 ± 1	99 ± 1	<0.0001	76 ± 7*	100 ± 0	100 ± 1	<0.0001

HR, heart rate; PaO_2, partial pressure of arterial oxygen; $PaCO_2$, partial pressure of arterial carbon dioxide; HCO_3, bicarbonate; SaO_2, arterial saturation

*$P < 0.05$ in comparison to the normal group

Table 3 Myocardial blood flow heterogeneity of the left and right ventricle in normal, hypoxic, and reoxygenated myocardium

Parameter	4 Weeks			8 Weeks		
	Cyanotic ($n = 6$)	Oxygenated ($n = 6$)	Normal ($n = 6$)	Cyanotic ($n = 6$)	Oxygenated ($n = 6$)	Normal ($n = 7$)
LV	0.529 ± 0.170	0.393 ± 0.072	0.520 ± 0.148	0.637 ± 0.099	0.477 ± 0.118	0.510 ± 0.060
P	0.08	—	0.08	0.03	—	0.25
RV	0.581 ± 0.175	0.446 ± 0.063	0.547 ± 0.163	0.631 ± 0.136	0.467 ± 0.056	0.575 ± 0.086
P	0.15	—	0.26	0.03	—	0.02

P values are versus the reoxygenation group

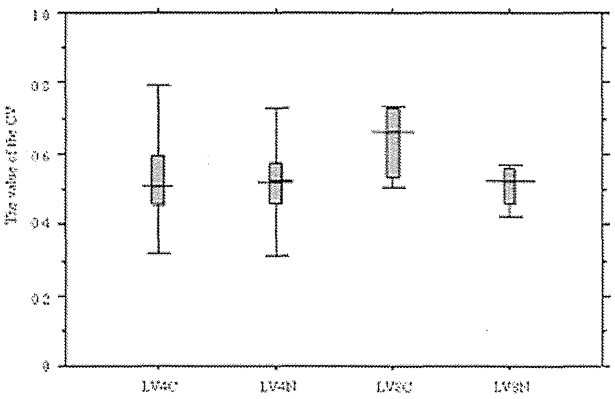

Fig. 2 Coefficients of variation (CV) of LV myocardial flow distribution in the cyanotic and control groups at 4 and 8 weeks of age. *Vertical bars* represent the standard deviations; *horizontal bars* across the boxes represent the median values. There was a trend toward a higher CV in the 8-week-old cyanotic rats than in age-matched control rats ($P = 0.06$)

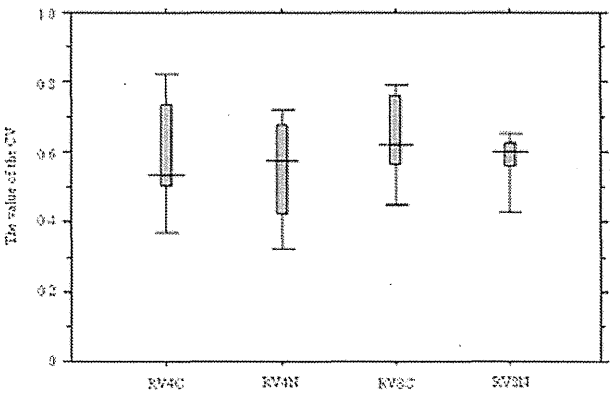

Fig. 3 Coefficients of variation (CV) of right ventricular (RV) myocardial flow distribution in the cyanotic and control groups at 4 and 8 weeks of age. *Vertical bars* represent the standard deviations; *horizontal bars* across boxes represent the median values

There was no significant difference in the CV of the LV myocardium (LVCV) between the cyanotic and control groups at 4 weeks of age (0.529 ± 0.170 vs. 0.520 ± 0.148) (Table 3; Fig. 2). There was a trend toward a higher LVCV in the cyanotic group than in the control group at 8 weeks (0.637 ± 0.099 vs. 0.510 ± 0.060, $P = 0.06$). No significant difference was found in the CV of the RV myocardium (RVCV) between the cyanotic and control groups at both 4 weeks of age (0.581 ± 0.175 vs. 0.547 ± 0.163, $P = 0.52$) and 8 weeks of age (0.631 ± 0.136 vs. 0.575 ± 0.086, $P = 0.48$) (Table 3; Fig. 3).

Age-related changes

The BW as well as the WH, LV, and RV weights increased with age in both groups (Table 1). The